Molecular Cell, Vol. 20, 929–938, December 22, 2005, Copyright ©2005 by Elsevier Inc. DOI 10.1016/j.molcel.2005.11.022

The SAXS Solution Structure of RF1 Differs from Its Crystal Structure and Is Similar to Its Ribosome Bound Cryo-EM Structure

Bente Vestergaard,[1,6] Suparna Sanyal,[2,6] Manfred Roessle,[3] Liliana Mora,[4] Richard H. Buckingham,[4] Jette S. Kastrup,[1] Michael Gajhede,[1] Dmitri I. Svergun,[3,5] and Måns Ehrenberg[2,*]

[1] Biostructural Research
Department of Medicinal Chemistry
Danish University of Pharmaceutical Sciences
Universitetsparken 2
DK-2100 Copenhagen
Denmark

[2] Department of Cell and Molecular Biology
Uppsala University, BMC
S-75124 Uppsala
Sweden

[3] European Molecular Biology Laboratory
Hamburg Outstation
D-22603 Hamburg
Germany

[4] UPR9073 du CNRS
IBPC
13 rue Pierre et Marie Curie
75005 Paris
France

[5] Institute of Crystallography
Leninsky pr. 59
117333 Moscow
Russia

Summary

Bacterial class I release factors (RFs) are seen by cryo-electron microscopy (cryo-EM) to span the distance between the ribosomal decoding and peptidyl transferase centers during translation termination. The compact conformation of bacterial RF1 and RF2 observed in crystal structures will not span this distance, and large structural rearrangements of RFs have been suggested to play an important role in termination. We have collected small-angle X-ray scattering (SAXS) data from *E. coli* RF1 and from a functionally active truncated RF1 derivative. Theoretical scattering curves, calculated from crystal and cryo-EM structures, were compared with the experimental data, and extensive analyses of alternative conformations were made. Low-resolution models were constructed ab initio, and by rigid-body refinement using RF1 domains. The SAXS data were compatible with the open cryo-EM conformation of ribosome bound RFs and incompatible with the crystal conformation. These conclusions obviate the need for assuming large conformational changes in RFs during termination.

Introduction

Stop codons entering the ribosomal decoding center (DC) during messenger RNA (mRNA) translation are recognized by class I release factors (RFs) that bind to the ribosomal A site and induce hydrolysis of the ester bond between the peptide chain and tRNA in the P site (reviewed by Kisselev et al. [2003]). In eubacteria, there are two class I RFs, RF1 and RF2, that recognize UAA and UAG or UAA and UGA, respectively (Scolnick et al., 1968). In eukaryotes or archaebacteria, one class-1 RF, eRF1 or aRF1, respectively, recognizes all three stop codons (Beaudet and Caskey, 1971). Archaebacterial and eukaryotic RFs are closely related in sequence but are almost unrelated to eubacterial RFs. One sequence motif alone is universally conserved, an essential GGQ tripeptide motif, believed to enter the peptidyl-transferase center (PTC) and trigger ester bond hydrolysis (Frolova et al., 1999). This is supported by experiments showing that mutations in the GGQ motif inhibit ester bond hydrolysis and peptide release but not RF binding to the A site of the ribosome (Seit Nebi et al., 2000; Zavialov et al., 2002). The tripeptide Q residue is N^5-methylated both in *eubacteria* (Dincbas-Renqvist et al., 2000; Heurgue-Hamard et al., 2002; Pannekoek et al., 2005) and in *S. cerevisiae* (Heurgue-Hamard et al., 2005), and this modification stimulates RF action (Dincbas-Renqvist et al. [2000] and V. Heurgue-Hamard, L.M., and R.H.B., unpublished data).

Genetic and biochemical evidence suggests that a unique peptide motif in bacterial RFs, PXT in RF1 and SPF in RF2 (Ito et al., 2000; Mora et al., 2003b), and two peptide motifs, NIKS and YXCXXXF in eRF1 and aRF1 (Frolova et al., 2002; Kisselev et al., 2003; Seit-Nebi et al., 2002; Song et al., 2000), recognize cognate stop codons by direct interaction with the mRNA in the A site. These observations suggest that RFs mimic tRNAs, both at the anticodon region and the aminoacyl-ACC terminus (Frolova et al., 1999; Ito et al., 2000), which would imply that the codon recognition motif and the GGQ motif should span the distance of 75 Å between the DC and the PTC of the ribosome, as do the anticodon and CCA ends of tRNAs (Kim et al., 1974; Suddath et al., 1974).

The crystal structure of human eRF1 (Song et al., 2000) is consistent with this constraint (Yusupov et al., 2001), but the distance between the SPF and GGQ motifs in the crystal structure of *E. coli* RF2 is only 23 Å (Vestergaard et al., 2001). This surprising result threw doubt on the prevailing interpretations of genetic and biochemical experiments in terms of known functional sites, and suggested that RFs in eukaryotes and eubacteria may function in significantly different ways. An equally short distance between the two motifs was subsequently found in crystal structures of RF1 from *T. maritima* (Shin et al., 2004) and *Streptococcus mutans* (accession number 1ZBT). This apparent dilemma was resolved by cryo-electron microscopic (cryo-EM) reconstructions of ribosome bound RF2 (Klaholz et al., 2003; Rawat et al., 2003). In the crystal structures of eubacterial RFs, a loop in domain II containing the SPF/PXT motif and a loop in domain III containing the GGQ motif are close together. Domains II and IV form a "core domain" II/IV and are firmly bound to each other by numerous hydrogen bonds, salt bridges, and hydrophobic

*Correspondence: ehrenberg@xray.bmc.uu.se
[6] These authors contributed equally to this work.

interactions (Kjeldgaard, 2003; Vestergaard et al., 2001). The core domain forms a large interface with domain III in this "closed conformation." In the cryo-EM structure of RF2, the core domain is similar to that in the crystal structure, with the SPF motif in the DC. However, the interface between the core domain and domain III is disrupted, and domain III has undergone a rotation of about 75° and points toward the PTC, thereby allowing the GGQ motif to reach the PTC. In this open conformation, the orientation of domain I with respect to the core domain is also modified, by a rotation of about 30°.

Assuming that the solution structures of eubacterial RFs are in the closed form as in the crystal structures, it was suggested (Rawat et al., 2003) that the RF enters the ribosome in the closed form and that a cognate interaction between the SPF/PXT motif and a stop codon might trigger a major conformational change to the open form. This mechanism is attractive in that it offers a structural explanation for how the cognate interaction between an RF and a stop codon might be signaled to the PTC by opening the RF structure to allow a direct interaction of the GGQ motif with the PTC while the core domain remains in the DC. It suggests, however, different principles for stop-codon recognition in eubacteria and in eukaryotes, since eRF1 shows no closed form either in the crystal or in solution, as determined by small-angle X-ray scattering (SAXS) (Kononenko et al., 2004). This would imply that stop-codon recognition must be signaled to the PTC in a way that is different from the mechanism proposed for RF1 and RF2 (Rawat et al., 2003). In view of the independent evolution of eubacterial and eukaryotic RFs, such a possibility could not be excluded.

Here we have used SAXS to test the hypothesis that the solution structure of RF1 from *E. coli* is closed, as in the crystal structure of RF1 or RF2. SAXS gives orientation-averaged information about the solution structures of molecules with sizes in the range of 1–100 nm (Koch et al., 2003). The approach can be used to evaluate whether any given structure of RF1 is compatible with the SAXS data and therefore with the authentic solution structure of the molecule (Svergun et al., 1995; Svergun, 1999). Since domain I of eubacterial RFs is likely to be flexible in solution, we have also analyzed a domain I-truncated variant of RF1 that is shown to be fully active in peptide release (Mora et al., 2003b). We conclude that the solution structure of RF1 is open, as in the cryo-EM structures of the eubacterial RFs, and not closed, as in their crystal structures. Our results suggest that stop-codon recognition and peptide release occur according to similar principles in eubacteria and eukaryotes, and, in the light of the new data, we discuss how premature peptide release may be avoided.

Results

Solution Structures of Full-Length and Truncated RF1 from *E. coli*

To study the solution structures of eubacterial RFs, we prepared solutions of full-length RF1 and RF2 from *E. coli* as well as of truncated variants of these factors lacking domain I. Monodisperse, concentrated solutions of full-length RF1 and its His-tagged truncated form dRF1 (residues 90–342, *E. coli* numbering) were obtained and used to collect SAXS data. Both the full-length and the truncated forms of RF1 were active in termination in vitro as well as in vivo (Mora et al., 2003a). Due to problems with precipitation, we were unable to obtain concentrated monodisperse solutions of either full-length or truncated RF2.

Molecular masses, estimated from the scattering curves for full-length RF1 (Figure 1A) and its truncated form dRF1 (Figure 1B), are in good agreement with the values computed from the corresponding sequences, as expected for monodisperse solutions. The radii of gyration (R_g) for RF1 and dRF1 were estimated from the scattering data (Figure 1) as 29 ± 1 Å and 26 ± 1 Å, respectively (see Figure 2). For comparison with the SAXS data, we designed a series of atomic models of full-length and truncated RF1 (Figure 3, also see Figure S1 with the Supplemental Data available with this article online), based on existing crystal and cryo-EM structures of RF1 and RF2. The crystal structures of RF1 (Shin et al., 2004) and RF2 (Vestergaard et al., 2001) are annotated RF1_XTb and RF2_XTa, respectively. Models obtained by superimposing the domains in the crystal structure of RF1 on the cryo-EM structure of RF1 (U. Rawat, H. Gao, A. Zavialov, R. Gursky, M.E., and J. Frank, unpublished data) on the cryo-EM structure of RF2 based on Klaholz et al. (2003) or on Rawat et al. (2003) are annotated RF1_EMc, RF1_EMa, or RF1_EMb, respectively. Finally, the model obtained by superimposing the domains of the crystal structure of RF1 (Shin et al., 2004) on the crystal structure of RF2 (Vestergaard et al., 2001) is annotated RF1_XTa. The corresponding truncated protein models lacking the N-terminal domain I (residues 1–89), were given the same names with "d" as prefix.

For both the full-length RF1 and its truncated variant, the R_g values estimated from the SAXS data are significantly larger than those computed from the crystallographic models, but they agree well with the R_g values computed from the cryo-EM models (Figure 2). This simple analysis, already pointing to a solution structure similar to the cryo-EM models, was extended and refined by comparing the experimental SAXS data with simulations of the full scattering patterns from the structural models by using the program CRYSOL (Svergun et al., 1995).

In general, the simulated SAXS curves from the models built on the closed conformation of either RF1 or RF2, as seen in their respective crystal structures, or built on molecular dynamics simulations (Ma and Nussinov, 2004) (see Table S1) fit poorly the experimental SAXS curves for both the full-length and truncated RF1. At the same time, the simulated SAXS curves from the models built on the open conformation of either RF1 or RF2, as seen in their cryo-EM structures, fit much better the experimental SAXS curves for full-length as well as truncated RF1 (Figures 1 and 2). The best fits of model-simulated and measured SAXS curves were obtained for the full-length (RF1_EMa) and truncated (dRF1_EMa) variants of the model, designed from one (Klaholz et al., 2003) (PDB accession code 1ML5, 21 Å resolution) of the two cryo-EM reconstructions of RF2 (Figures 3B, 1 and 4A). The models ([d]RF1_EMc) based on the cryo-EM reconstruction of RF1 (U. Rawat, H. Gao, A. Zavialov, R. Gursky, M.E., and J. Frank, unpublished data; resolution 12.8 Å) gave similar goodness of fit to

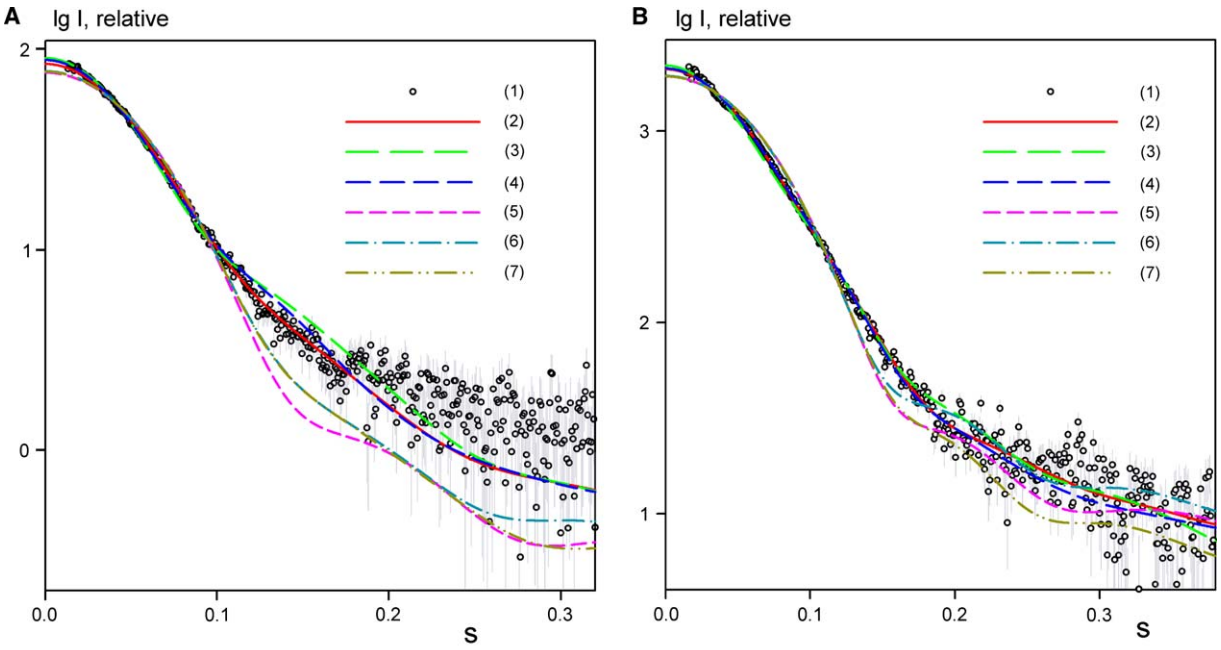

Figure 1. Fits between Models Derived from Experimentally Determined Structures of RFs and Solution Scattering Data of Truncated and Full-Length RF1

SAXS data from RF1 (A) and dRF1 (B), representing the logarithm of the intensity as a function of the momentum transfer $s = 4\pi \sin\theta/\lambda$, where 2θ is the scattering angle and λ is the wavelength. (1) Experimental scattering patterns; (2–7) computed scattering curves from the models (d)RF1_EMa, (d)RF1_EMb, (d)RF1_EMc, (d)RF1_XTa, (d)RF1_XTb, and (d)RF2_XTa, respectively.

the SAXS data, and the models ([d]RF1_EMb) designed from the other cryo-EM reconstruction of RF2 (Rawat et al., 2003) (PDB accession code 1MI6, resolution 12.8 Å) also fit the SAXS data quite well. We note that the fits of simulated to measured SAXS curves were significantly better for the hexa-His-tagged than for the untagged versions of the models (see Supplemental Data for details).

We have also used the simulated annealing-based modeling program DAMMIN (Svergun, 1999) for ab initio solution structure determination from SAXS data for both full-length and truncated RF1. The 15 best models for each data set (which neatly fit the experimental data with discrepancy $\chi = 1.25$ for dRF1 and $\chi = 0.85$ for RF1) were compared to the conformation of RF1 in the crystal structure ([d]RF1_XTb) and to the cryo-EM models (d)RF1_EMa. The normalized spatial discrepancies (NSD) between ab initio models and experimental structures (Kozin and Svergun, 2001) were consistently smaller for the cryo-EM structure (mean values 1.3–1.4 and 1.6–1.7 for the open and closed forms, respectively). For both types of discrepancy, between the experimental and calculated scattering curves (χ) and between the low- and high-resolution three-dimensional models (NSD), values around 1 indicate good agreement, and the higher the value, the worse the agreement (see definitions in Experimental Procedures). This means that the ab initio modeling restores the open and not the closed conformation (see also Table S2 and Figure S2 for details). Taken together, these data strongly suggest that full-length and truncated RF1 are present in solution in the open conformation seen by cryo-EM when RF2 (Klaholz et al., 2003; Rawat et al., 2003) or RF1 (U. Rawat, H. Gao, A. Zavialov, R. Gursky, M.E., and J. Frank, unpublished data) are bound to the ribosome, rather than the closed conformation seen in the crystal structures of RF2 (Vestergaard et al., 2001) and RF1 (Shin et al., 2004). Below we shall discuss the extent to which this conclusion might be influenced by possible flexibility and multiple conformations of the protein in solution.

Generation, Inspection, and Analysis of Random Models

In all structure determinations of eubacterial RFs up to now, domain I has appeared in different orientations in relation to the core domain II/IV (Klaholz et al., 2003; Ma and Nussinov, 2004; Rawat et al., 2003; Shin et al., 2004; Vestergaard et al., 2001) (also in U. Rawat, H. Gao, A. Zavialov, R. Gursky, M.E., and J. Frank, unpublished data). This is in line with the observation that domain I is loosely connected with the core domain II/IV via a loop region in both RF1 (Shin et al., 2004) and RF2 (Vestergaard et al., 2001). Furthermore, domain III adopts slightly different conformations in the two crystal structures, and its orientation in relation to the core domain II/IV differs for the cryo-EM reconstructions of RF1 (U. Rawat, H. Gao, A. Zavialov, R. Gursky, M.E., and J. Frank, unpublished data) and RF2 (1ML5 [Klaholz et al., 2003] and 1MI6 [Rawat et al., 2003]) on the posttermination ribosome. Hence, it is conceivable that both domains I and III of full-length RF1 in solution can adopt conformations different from those observed in any of the experimentally determined structures of RF1 and RF2. The possibility to model the solution structure with two potentially flexible domains creates an ambiguity in the interpretation of the SAXS data (see Table S1 and Supplemental Discussion online). Since domain I is lacking in the truncated but fully active dRF1 variant,

A

Model	χ	Rg Å
dRF2_Xta	3,26	22.20
dRF1_Xta	3,25	22.23
dRF1_XTb	2,97	23.68
dRF1_EMa	1,39	25.83
dRF1_EMb	1,97	27.90
dRF1_EMc	1,40	25.85
dRF1_DAM	1,25	26,80
RF2_Xta	2,38	25.42
RF1_Xta	2,67	25.13
RF1_XTb	2,30	25.53
RF1_EMa	1,12	27.96
RF1_EMb	1,55	29.91
RF1_EMc	1,26	30.21
RF1_DAM	0.85	30.40
Data set		
dRF1		26 +/-1
RF1		29 +/-1

B

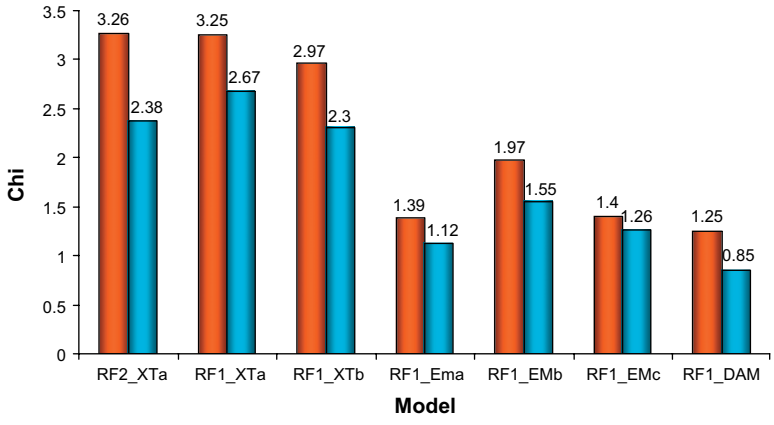

Figure 2. χ and R_g Values for Experimentally Based Models of dRF1 and RF1

(A) Table of the discrepancy χ and the radius of gyration R_g. When the discrepancy χ is close to 1, there is good agreement between experimental and calculated scattering curves. When χ is larger, the agreement is worse. R_g values were estimated from experimental scattering curves and from structural models. (B) Graphical representation of χ values versus experimental models. Blue, fits between truncated hexa-His-tagged models and data from truncated protein; orange, fits between full-length models and data from full-length protein. Values are marked above columns.

this type of ambiguity in the interpretation of the scattering data is absent. Therefore, SAXS data from truncated dRF1 were first used to determine the orientation of domain III in relation to the rigid core domain II/IV. For this, 200 models of dRF1 with domain III in random orientations were generated, including closed and open conformations of dRF1 (see Figure S1A), and their simulated SAXS curves were compared with the experimentally determined SAXS curves. Only six out of these 200 random dRF1 models generated scattering curves that fit the experimental data in the same range as the scattering curves generated by the three cryo-EM models (dRF1_EMa, dRF1_EMb, or dRF1_EMc), and all six had an open conformation with domain III separated from the core domain II/IV (Figure 4B). Notably, none of the scattering curves computed from the random dRF1 models yielded a better fit than the scattering curve from the dRF1_EMa model (Figures 2 and 4B).

To test if the experimental SAXS data originated from a mixture of molecules with domain III in different conformations, we also simulated the SAXS curve that would emerge if the 200 random model structures were simultaneously present in equal amounts in solution, by averaging the 200 simulated SAXS curves, and found a poor fit to the experimental scattering curve (Figure 5). From this, we suggest that domain III does not move freely in relation to the core domain II/IV in the solution structure of dRF1.

These results strongly support the notion that truncated dRF1 and, by inference, full-length RF1 have open conformations in solution. They also suggest that domain III in dRF1 and RF1 is oriented as in the dRF1_EMa model. Accordingly, for further analyses of data from the full-length RF1 solutes, domain III was subsequently fixed in this orientation in models of full-length RF1, while the orientation of domain I was chosen randomly in a set of 100 models, well covering the three-dimensional space (see Figure S1B online and Experimental Procedures for details). In this set, a large number of models gave rise to scattering curves that fitted well with the experimental SAXS curve from RF1, and some fits were even better than the one obtained from the RF1_EMa model. These models have domain I in very different orientations (Figure 4C), suggesting that domain I may be flexible in solution. An average scattering curve, based on all 100 models with greatly varying orientations of domain I (Figure 4C and Figure S1A), was calculated and compared to the experimental SAXS curve for RF1. The

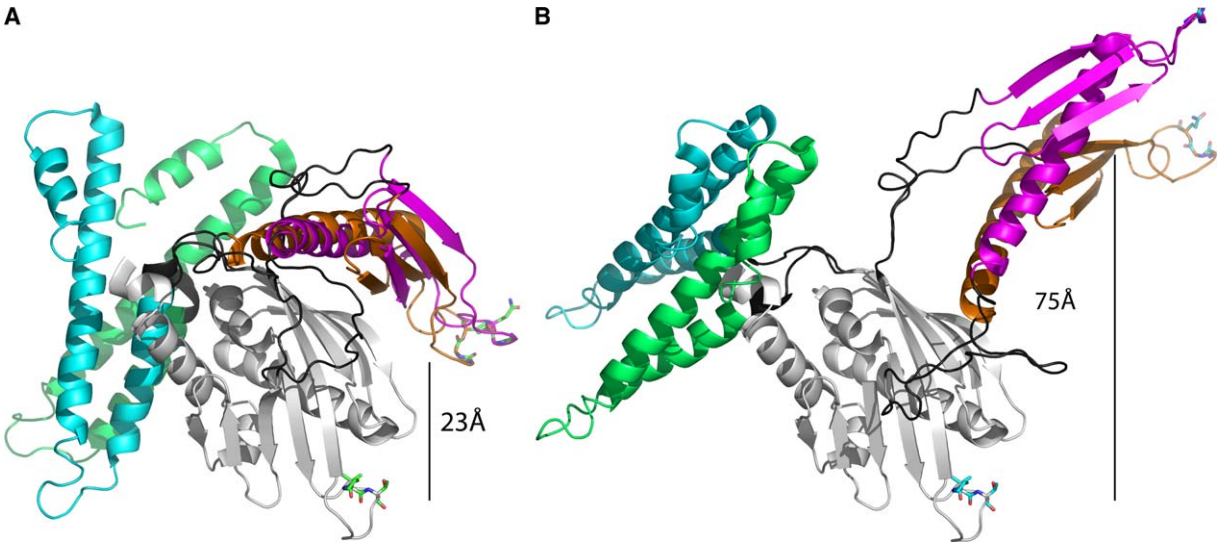

Figure 3. Representatives for Classes of Models Fitted to the Solution Scattering Data

All models are superimposed on the core domain II/IV, shown in off white. (A) Models of full-length RF1 based on the crystal structure of RF1 (model RF1_XTb, domain I is green, domain III is orange) and RF1 domains superimposed on the crystal structure of RF2 (model RF1_XTa, domain I is cyan, domain III is magenta). The GGQ and PAT motifs are shown as green atomic bond models, and the approximate distance is marked. The linkers that were flexible during the generation of random models are shown in dark gray. (B) Models of full-length RF1 based on the two cryo-EM reconstructions of RF2 (model RF1_EMa, domain I is green, domain III is orange; model RF1_EMb, domain I is cyan, domain III is magenta). Linkers are dark gray, and GGQ/PAT motifs are shown as blue atomic bond models. The figure was produced using Pymol (DeLano, 2002).

fit was excellent, with discrepancy $\chi = 1.07$, even better than $\chi = 1.12$, obtained for the RF1_EMa model (Figure 5). This is compatible with the view that domain I is highly flexible in solution, but does not exclude a fixed orientation. A list of the χ values obtained for the 100 models with domain I in randomly chosen orientations is provided as Table S1.

Rigid-Body Refinements

In an independent approach, a model of RF1 in solution was generated by rigid-body refinement from the high-resolution structures of the individual domains. The program SASREF (Petoukhov and Svergun, 2005) uses simulated annealing to find an optimal configuration of the domains by simultaneous fitting of the SAXS data from the full-length and the truncated protein. On the assumption that the structure of the truncated dRF1 is maintained in the full-length RF1, this approach excludes those compensatory changes in domains I and III that could have occurred if the rigid-body refinement were based only on the full-length RF1 data. Several independent SASREF runs, starting from different initial

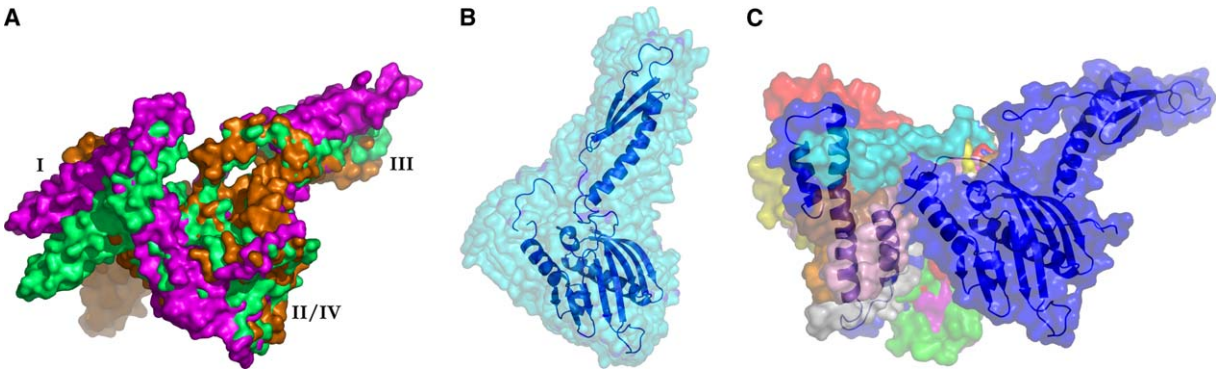

Figure 4. Superposition of the Best-Fit Models

(A) The models RF1_EMa (green) and RF1_EMb (magenta) and the simulated annealing result from SASREF (orange) in surface representation. The models are superimposed using Cα positions of all residues in domains II-III-IV. It is evident that the models mainly differ in the positions of domain I, explaining why all three models fit well to the SAXS curve. The positions of domains are labeled.

(B) Superposition on all Cα positions of the ten best-fitting random models of dRF1, shown as transparent surface representations in cyan. A cartoon representation of one model is shown in blue. The χ values for the fit to the experimental SAXS curve is between 1.4 and 1.6. All best-fitting models have approximately the same orientation of domain III.

(C) Transparent surface representations of the ten best-fitting random models of full-length RF1, superimposed using domains II/III/IV (shown in blue). In each of the ten models, domain I has been colored differently to emphasize the very different positions of this domain. One model is also represented as a cartoon (blue). χ values for the fit to the experimental SAXS curve lie between 0.97 and 1.07 and are thus as good as any of the experimentally derived models. The figure is made using Pymol (DeLano, 2002).

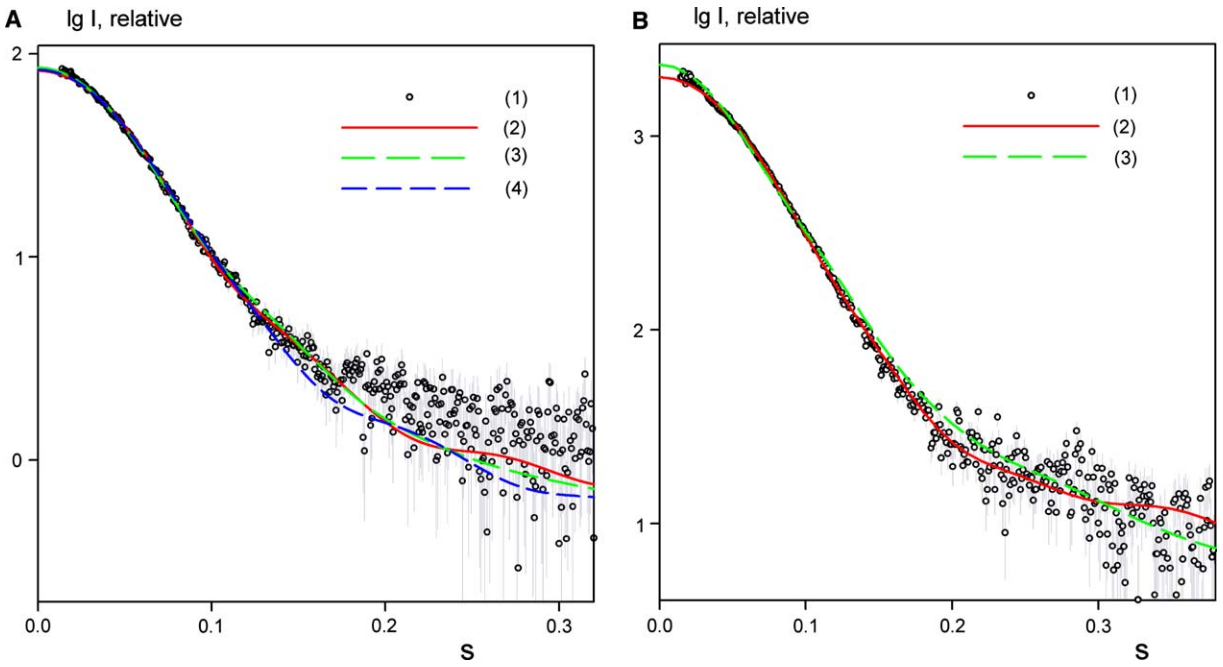

Figure 5. Simulation of Domains Flexible in Solution

SAXS data from RF1 (A) and dRF1 (B). (1) experimental scattering patterns (axes as in Figure 1), (2) scattering curves from the rigid-body model provided by SASREF, (3) averaged scattering over 200/100 generated models starting from the EMa model of dRF1/RF1. For full-length RF1, the averaged scattering from the models generated based on the crystallographic model with domain III in the closed conformation is given by curve (4).

configurations, converged to models very similar to the open conformation observed for the ribosome bound forms of RF1 and RF2 as observed by cryo-EM. These models (Figure 4A) provide fits to the experimental data from truncated and full-length RF1 with typical values of $\chi = 1.47$ and $\chi = 1.13$, respectively, close to the fits obtained for the models dRF1_EMa and RF1_EMa with χ values of 1.39 and 1.12, respectively. The resulting RF1 model is in an open conformation comparable to the cryo-EM models (Figure 4A). Thus, the SASREF approach gives further support to the conclusion that the solution structure of RF1 is open.

Oligomer Analysis of a Possible Mixture of the Closed and Open Forms

The program OLIGOMER (Konarev et al., 2003) was used to analyze whether the dRF1 solute contained a mixture of the closed and open forms. A marginally improved χ value of 1.37 (compared to 1.39 for the open form alone) was obtained by combining 7.5% of the closed form with 92.5% of the open form. This marginal improvement indicates that effectively no dRF1 is present in the closed conformation and, thus, that a putative equilibrium between the closed and open forms would be shifted almost entirely toward the open conformation (Figure 6).

Peptide Release Activity of dRF1

Previous experiments showed that dRF1 is able to complement a thermosensitive mutant of RF1 when produced from a plasmid at the nonpermissive temperature of 42ºC (Mora et al., 2003a). In view of the significance of dRF1 for the SAXS studies reported here, the activity of the truncated factor has been studied more closely by deleting the chromosomal copy of *prfA* and making cell survival entirely dependent on expression of dRF1 from an inducible promoter ahead of the gene encoding dRF1 on a plasmid. In the absence of the inducer IPTG, cell growth was very slow (about 10% of wild-type). With a low level of induction in the presence of 10^{-5} mM IPTG, cell growth on rich solid medium at 37ºC was indistinguishable from that of normal cells (data not shown), indicating that dRF1 can functionally replace the normal factor. Cell growth was cryosensitive, a phenotype also shown by *prfC*-inactivated mutants, which lack the class II release factor RF3 catalyzing the recycling of class I RFs (Ehrenberg et al., 2000). It is possible that the cryosensitivity is the result of slow recycling of dRF1, which would be consistent with the fact that N-terminal truncation of RF1 removes the domain interacting with RF3 (Mora et al., 2003b).

Discussion

SAXS data provide rotationally averaged scattering profiles (Svergun et al., 1995; Svergun, 1999) and can be used to discriminate between preexisting protein models with sufficiently large differences in their tertiary structures by comparing calculated and observed scattering profiles. This strategy, supported by model independent ab initio solution structure determination (Svergun, 1999) and rigid-body modeling (Petoukhov and Svergun, 2005), was used to characterize the solution structures of full-length and domain I-truncated variants of the eubacterial release factor 1 (RF1). Our results show these structures to be in open conformations, in which domain III is separated from the core domain II/IV. This result is surprising, since it implies that the

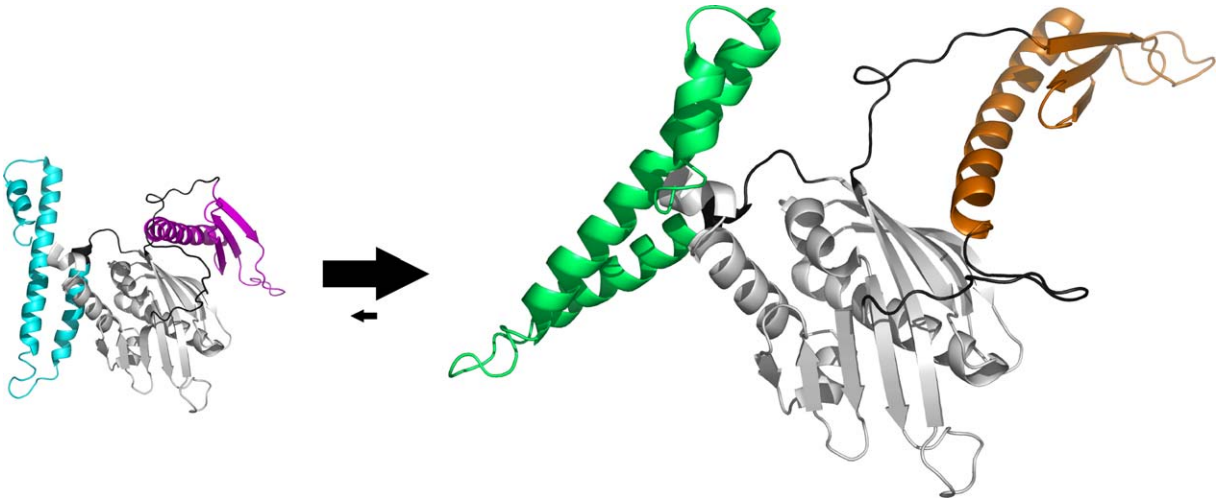

Figure 6. Equilibrium Shifted toward the Open Form

Illustration of the equilibrium between the open and the closed conformation in solution. The majority of RFs are in the open conformation but can exist in the closed conformation. The presence of hydrophobic residues in the interface between domains III and the core domain II/IV may be important for this equilibrium. Models are of the best-fitting model of RF1 (based on the 21 Å resolution cryo-EM reconstruction of RF2 [right, PDB code 1ML5 (Klaholz et al., 2003)], domain I is green, domain III is orange) and the crystal structure of RF1 (left, PDB code 1RQ0 [Shin et al., 2004], domain I is turquoise, domain III is magenta). The core domain II/IV is colored in cream. The figure was produced in Pymol (DeLano, 2002).

solution structure of RF1 and, by tentative inference, the solution structure of RF2 are open, in contrast to the crystal structures of RF1 (Shin et al., 2004) and RF2 (Vestergaard et al., 2001), in which domain III forms an interface with the core domain II/IV. Instead, the solution structure of RF1 appears to be very similar to the ribosome bound cryo-EM structures of RF1 (U. Rawat, H. Gao, A. Zavialov, R. Gursky, M.E., and J. Frank, unpublished data) and RF2 (Klaholz et al., 2003; Rawat et al., 2003), which all have open conformations. It should be stressed that the open conformation is clearly inferred from independent analysis of the scattering from RF1 and dRF1, so that the full-length and deletion mutant data complement and corroborate each other.

Our analysis was extended by simulating SAXS curves from a large number of structural models in which domains I and III were allowed to adopt random orientations in relation to the core domain II/IV. This approach made it possible to probe putative flexibilities of domains I and III in the solution structure of RF1, and to test possible structures other than the previously reported structures of RFs, as determined by X-ray crystallography or cryo-EM. The results of this analysis are inconsistent with a large degree of flexibility for domain III but suggest that domain I can move quite freely with respect to the core domain II/IV. In the cryo-EM reconstructions, which first described the open conformation, the domains from the crystal structures were superimposed onto the cryo-EM electron density, using loops from the crystal structures as hinge regions. The resolution of cryo-EM does not allow for assignment of putative newly formed secondary structure elements, like α helices, formed in the hinge regions during the transition from the closed crystal to the open forms of RF1 and RF2, and they also remain unassigned in the present analysis of the solution structure of RF1. Nevertheless, our conclusion that domain III has a fixed orientation in relation to the core domain II/IV in the open solution structure of RF1 suggests a stabilization of this conformation by as-yet-unknown secondary structure elements other than the loop regions.

The present observations suggest that the distance between the GGQ motif and the stop-codon-recognizing motif of each one of the eubacterial RFs is close to 75 Å already in their solution structures. Therefore, they are able to span the distance between the ribosomal DC and PTC without any conformational change of the RF upon ribosome binding. The distance between the NIKS motif involved in stop-codon recognition, and the GGQ motif in the crystal structure of the eukaryotic release factor 1 (eRF1), is about 80 Å (Song et al., 2000), suggesting that eRF1 can also span the distance between the DC and the PTC without a major conformational change when it binds to the ribosome. If so, this would imply that the mechanisms for ribosome binding and codon recognition by eubacterial and eukaryotic RFs may, after all, be similar, in contrast to the earlier conclusion based on their strikingly different crystal structures (Vestergaard et al., 2001).

Previously, we suggested how the cognate interaction between a stop codon in the ribosomal DC and a eubacterial RF is signaled to the ribosomal PTC by a conformational change of the RF from its closed to its open form, thereby bringing the GGQ motif in contact with the ribosomal PTC (Rawat et al., 2003). Taken at face value, the present results refute this hypothesis. If, as we have found here, the solution structure of RF1 is like its ribosome bound form, then the "signaling" must work according to a different principle. It is essential for RF and tRNA selection by codon-programmed ribosomes that the accuracy of codon recognition is not wasted by too slow a release of factor or tRNA after the first binding event (Ehrenberg and Kurland, 1984; Kurland and Ehrenberg, 1987; Ninio, 1974). We have found very slow, spontaneous dissociation of RF1 and RF2 from the posttermination ribosome (Freistroffer et al., 1997; Zavialov et al., 2001; Zavialov et al., 2002). If dissociation of the RFs is equally slow from pretermination ribosomes

before hydrolysis of the ester bond between the peptide chain and the P site tRNA, this would inevitably lead to a high frequency of erroneous termination events with sense codons in the DC. Since, however, RF1 and RF2, in spite of the absence of proofreading, discriminate extremely well against sense codons (Freistroffer et al., 2000), we suggest that they dissociate much more rapidly from the pretermination than from the posttermination ribosome, but by another and perhaps less conspicuous mechanism than the one previously proposed (Rawat et al., 2003).

The crystal structures of RF1 (Shin et al., 2004) and RF2 (Vestergaard et al., 2001) were obtained independently from factors purified from two different organisms and appeared in different crystal forms. Their closed crystal forms, very different from the solution structure of RF1, may thus have been favored in the crystal lattices (Andersson and Hovmoller, 2000). The present analysis shows that, if there is equilibrium between open and closed conformations of RF1 (Figure 6) in solution, it must be shifted almost completely toward the open form. In the closed crystal structures of RF1 and RF2, there is an interface between domain III and the core domain II/IV containing hydrophobic residues that are exposed to the solvent in the open form of the factors. In the RF2 family, several of these hydrophobic residues (226, 230, 264, 270, and 298; *E. coli* RF2 numbering) are conserved. There are only two conserved residues of this type in RF1 (89 and 193; *T. maritima* RF1 numbering), although additional hydrophobic but nonconserved residues (140, 142, 186, and 191) are located in the domain interface of *T. maritima* RF1.

The fact that we could obtain monodisperse solutions of RF1 but not of RF2 might be explained by the different sets of hydrophobic amino acids that become exposed during the transition from closed to open conformations of these proteins. The present results raise the question as to whether the crystal structures of RF1 and RF2 reflect a functional state of the factors or whether they occur only in the crystals and are without biological significance. Recent crystallographic data show that *E. coli* RF1 in complex with the RF methyltransferase PrmC does adopt a closed conformation and thus support the idea that this form is functionally relevant (Graille et al., 2005).

In summary, RF1 exists in solution in an open conformation, with domain III in a fixed orientation separated from the core domain II/IV as in the cryo-EM reconstructions of the eubacterial RFs (Klaholz et al., 2003; Rawat et al., 2003) (and U. Rawat, H. Gao, A. Zavialov, R. Gursky, M.E., and J. Frank, unpublished data). Our data are compatible with domain I being either flexible or held in a fixed orientation in relation to domains II/IV and III in the solution structure of RF1. Our results radically change current views regarding the mechanism of termination of eubacterial protein synthesis.

Experimental Procedures

Sample Preparation

E. coli RF1 was purified from an overproducing strain as previously described (Dincbas et al., 1999). Truncated His-tagged *E. coli* RF1 was purified as described (Mora et al., 2003b), with the following modifications: cultures of transformed cells were grown in LB, ampicillin (200 μg/ml) at 42°C to an OD_{600} of 0.5. At 14°C, the cells were induced with 1 mM IPTG and incubated for 15 hr. After cell lysis and purification of dRF1 on Ni chelation resin (Sigma), the protein was subjected to partial ammonium sulfate precipitation in the range of 1–2 M $(NH_4)_2SO_4$, redissolved at a concentration of 7 mg/ml in buffer (20 mM Tris-HCl [pH 7.5], 100 mM NaCl), and immediately purified by size exclusion in the same buffer. Eluting 0.5 ml fractions were kept separate for the SAXS data collection. Finally, the purified proteins were dialysed against the size exclusion buffer. For full-length RF1, 2 mM $MgSO_4$ and 1 mM DTE were added. All chemicals were of analytical grade.

Data Collection and Initial Data Treatment

The synchrotron SAXS data were collected on the X33 camera of the European Molecular Biology Laboratory on the storage ring DORIS III (DESY, Hamburg, Germany [Koch and Bordas, 1983]). Scattering from RF1 protein solutions with concentrations between 1 and 10 mg/ml was measured at 20°C at a wavelength of $\lambda = 0.15$ nm, using a linear gas detector (Gabriel et al., 1994), in the momentum transfer range $0.01 < s < 0.35$ Å^{-1} ($s = 4\pi \sin\theta/\lambda$, where 2θ is the scattering angle). dRF1 samples were measured at concentrations between 1 and 3 mg/ml at 4°C and 20°C, using a MAR345 Image Plate detector, in the momentum transfer range $0.01 < s < 0.45$ Å^{-1}. Repetitive exposures of the same protein solution performed in 1 and 5 min time frames for the gas and Image Plate detector, respectively, indicated no changes in the scattering patterns with time, i.e., there was no measurable radiation damage for the RF1 and dRF1 samples. The data were normalized to the intensity of the transmitted beam and corrected for the detector response, and the difference curves after buffer scattering subtraction were extrapolated to infinite dilution using the program PRIMUS (Konarev et al., 2003). The radii of gyration R_g were evaluated by the program GNOM (Svergun, 1992; Svergun et al., 1988). The molecular masses of the solutes were estimated by comparing the extrapolated forward scattering I(0) with that of a reference solution of bovine serum albumin.

Modification of Initial Test Models

Structural water molecules were removed from the 1.8 Å crystal structure of *E. coli* RF2 (PDB code 1GQE) (Vestergaard et al., 2001), resulting in the model named RF2_XTa. Missing residues (A208-A211, A269-A278, and A334-A342) in the 2.65 Å *T. maritima* RF1 crystal structure (PDB code 1RQ0, molecule A) (Shin et al., 2004) were modeled based on the crystal structure of RF2 (Vestergaard et al., 2001). Although invisible in the crystal structure, these residues contribute to the SAXS. This model is denoted RF1_XTb and has *E. coli* RF1 sequence.

The domains from RF1_XTb were superimposed onto the RF2 crystal structure, resulting in the model RF1_XTa. The domains were also superimposed on the cryo-EM models of ribosome bound RF2 obtained at 21.0 Å (Klaholz et al., 2003) and 12.8 Å (Rawat et al., 2003) resolution (PDB codes 1ML5 and 1MI6), and these models are named RF1_EMa and RF1_EMb, respectively. Coordinates of the 12.8 Å resolution reconstruction of ribosome bound RF1 were modified to include residues 208–216 and 269–278, and resulted in the RF1_EMc model (U. Rawat, H. Gao, A. Zavialov, R. Gursky, M.E., and J. Frank, unpublished data).

Coordinates representing two molecular dynamics simulations of RF2 (Ma and Nussinov, 2004) were kindly provided by Professor Byuong Ma. Models of the truncated factors were made by deleting domain I from the above models (residues 1–89, *E. coli* RF1 numbering), with and without a modeled C-terminal hexa-His-tag (green in Figure S1A). All models were made using the program O (Jones and Kjeldgaard, 1997).

Ab Initio Modeling

The ab initio program DAMMIN (Svergun, 1999) employs simulated annealing to reconstruct the particle shape at low resolution by searching for a compact bead model minimizing the discrepancy between the experimental curve and that calculated from the model

$$\chi^2 = \frac{1}{N-1}\sum_j \left[\frac{I_{\exp}(s_j) - cI_{calc}(s_j)}{\sigma(s_j)}\right]^2 \quad (1)$$

where N is the number of data points and c is a scaling factor. $I_{exp}(s_j)$, $I_{calc}(s_j)$, and $\sigma(s_j)$ are the experimental intensity, the calculated intensity, and the experimental error at the momentum transfer s_j,

respectively. Fifteen independent bead models for both truncated and full-length protein were compared to the models (d)RF1_EMa and (d)RF1_XTa by the program SUPCOMB (Kozin and Svergun, 2001). This program automatically aligns two arbitrary three-dimensional models (in this case, a low-resolution ab initio model with either a high-resolution crystallographic or a cryo-EM model) by minimizing the normalized spatial discrepancy, which also provides a quantitative measure of agreement between the two three-dimensional models (Kozin and Svergun, 2001).

Generation of Random PDB Models

Random models were generated using the program CNS (Brunger et al., 1998). The script "anneal.inp" was modified to exclude energy contributions from diffraction data. Torsion angle molecular dynamics simulations were performed, and the number of molecular dynamics steps at the initial temperature was increased from the default six to 100 steps. The initial temperature was set to 30,000 K, and a cooling rate of 100 K per step was used. To generate models of dRF1 with domain III movements, only linkers (residues 184–196 and 266–281, Figures 3A and 3B) connecting domain III to the core domain II/IV were modified, resulting in rigid-body movements of domain III (residues 197–265). One hundred models were generated using dRF1_EMa as the starting model. An additional 100 models were made using dRF1_XTa as the starting model. To generate 100 models of full-length RF1 with domain I movements, residues 1–77 were defined as a rigid body moving at the end of a nine residue linker (residues 78–86; Figures 3A and 3B), while the remaining part of the structure was kept fixed in the position corresponding to dRF1_EMa. See Supplemental Discussion for additional analysis of alternative models.

Data Analysis and Generation of a Solution Structure

The SAXS patterns from the atomic structures and models were calculated with the program CRYSOL (Svergun et al., 1995). For simulating a flexible domain III in dRF1 or a flexible domain I in RF1, the theoretical averaged scattering intensities from the CRYSOL output files for each class of models were calculated and fitted to the experimental data.

For the rigid-body modeling of RF1/dRF1, the scattering amplitudes from the individual domains were calculated using CRYSOL, and positions of the core domain II/IV were fixed (domain borders as above). The program SASREF (Petoukhov and Svergun, 2005) employs a simulated annealing protocol performing random movements/rotations of domains I and III while requiring polypeptide chain connectivity and avoiding steric clashes. At each simulated annealing step changing the positions of domain I or III as rigid bodies, scattering from the full-length model and the domain I-truncated model was computed to ultimately simultaneously fit the two scattering curves from RF1 and dRF1.

Cell Growth Dependent on dRF1

The *prfA* gene on the chromosome was inactivated by insertion of a *tetR-tetA* cassette, essentially as described for the inactivation of *prfB* (Mora et al., 2003b). Homologous recombination with linear DNA in a recombination-proficient strain (Yu et al., 2000) expressing wild-type RF1 from a plasmid resulted in the deletion of *prfA* and the downstream *prmC* gene becoming expressed from the *tetA* promoter. The *prfA* region was transduced with phage P1 to strains expressing dRF1 from a plasmid, under the control of the IPTG inducible *trac* promoter (Mora et al., 2003b).

Supplemental Data

Supplemental Data include two figures, two tables, Supplemental Discussion, and Supplemental References and can be found with this article online at http://www.molecule.org/cgi/content/full/20/6/929/DC1/.

Acknowledgments

Dr. Thomas Hamelryck is thanked for help with rewriting of the CNS input-file anneal.inp and automating CRYSOL analysis. Dr. Bouyong Ma is acknowledged for providing coordinates of the molecular dynamics simulation of RF2. We thank Dr. Michel Koch for his help with initial RF1 SAXS data collection. This work was supported by the Centre National de la Recherche Scientifique (UPR9073), l'Association pour la Recherche sur le Cancer, the Fondation pour la Recherche Medicale (L.M. and R.H.B.), the Lundbeck Foundation (B.V.), the Danish Natural Science Foundation (B.V.), DANSYNC (B.V., J.S.K., and M.G.), and the Swedish National Research Council Grants to M.E. (621-2003-2832) and S.S. (621-2002-4747) and National Institute of Health Grant GM70768 (to M.E. and S.S.). We acknowledge the support of the European Community-Research Infrastructure Action under the FP5 "Improving Human Potential Programme (HPRI-CT-1999-00017)" and under the FP6 "Structuring the European Research Area Programme (RII3/CT/2004/5060008)" to the EMBL Hamburg Outstation to cover the expenses for travel and accommodation of S.S. at EMBL Hamburg. B.V. has contributed with purification of truncated protein, data collection, generation of random models, solution structure determination, and main manuscript preparations. S.S. has contributed with purification of full-length protein, data collection, fitting of random models, solution structure determination, and manuscript preparation. J.S.K. and M.G. have contributed with scientific discussions, computing, and writing of the manuscript. M.R. and D.I.S. have contributed in SAXS experiments and data analysis. L.M. and R.H.B. constructed RF1 and dRF1 overproducing plasmids, overproduced truncated RF1, constructed prfA deleted strain, and characterized the strain in vivo for its dependence on truncated RF1 for survival. M.E. identified the scientific problem and suggested the experimental strategies, functioning as principal investigator and project leader.

Received: October 12, 2005
Revised: November 15, 2005
Accepted: November 28, 2005
Published: December 21, 2005

References

Andersson, K.M., and Hovmoller, S. (2000). The protein content in crystals and packing coefficients in different space groups. Acta Crystallogr. D Biol. Crystallogr. *56*, 789–790.

Beaudet, A.L., and Caskey, C.T. (1971). Mammalian peptide chain termination. II. Codon specificity and GTPase activity of release factor. Proc. Natl. Acad. Sci. USA *68*, 619–624.

Brunger, A.T., Adams, P.D., Clore, G.M., DeLano, W.L., Gros, P., Grosse-Kunstleve, R.W., Jiang, J.S., Kuszewski, J., Nilges, M., Pannu, N.S., et al. (1998). Crystallography & NMR system: a new software suite for macromolecular structure determination. Acta Crystallogr. D Biol. Crystallogr. *54*, 905–921.

DeLano, W.L. (2002). The PyMOL Molecular Graphics System (San Carlos, CA: DeLano Scientific).

Dincbas, V., Heurgue-Hamard, V., Buckingham, R.H., Karimi, R., and Ehrenberg, M. (1999). Shutdown in protein synthesis due to the expression of mini-genes in bacteria. J. Mol. Biol. *291*, 745–759.

Dincbas-Renqvist, V., Engstrom, A., Mora, L., Heurgue-Hamard, V., Buckingham, R., and Ehrenberg, M. (2000). A post-translational modification in the GGQ motif of RF2 from *Escherichia coli* stimulates termination of translation. EMBO J. *19*, 6900–6907.

Ehrenberg, M., and Kurland, C.G. (1984). Costs of accuracy determined by a maximal growth rate constraint. Q. Rev. Biophys. *17*, 45–82.

Ehrenberg, M., Andersson, K., Dincbas, V., Freistroffer, D., Heurgué-Hamard, V., Karimi, R., Pavlov, M., and Buckingham, R.H. (2000). The mechanism of prokaryotic translation termination and ribosome recycling. In The Ribosome: Structure, Function, Antibiotics and Cellular Interactions, R.A. Garrett, S.R. Douthwaite, A. Liljas, A.T. Matheson, P.B. Moore, and H.F. Noller, eds. (Washington, D.C.: ASM, Blackwell Science), pp. 541–551.

Freistroffer, D.V., Pavlov, M.Y., MacDougall, J., Buckingham, R.H., and Ehrenberg, M. (1997). Release factor RF3 in *E. coli* accelerates the dissociation of release factors RF1 and RF2 from the ribosome in a GTP-dependent manner. EMBO J. *16*, 4126–4133.

Freistroffer, D.V., Kwiatkowski, M., Buckingham, R.H., and Ehrenberg, M. (2000). The accuracy of codon recognition by polypeptide release factors. Proc. Natl. Acad. Sci. USA *97*, 2046–2051.

Frolova, L.Y., Tsivkovskii, R.Y., Sivolobova, G.F., Oparina, N.Y., Serpinsky, O.I., Blinov, V.M., Tatkov, S.I., and Kisselev, L.L. (1999).

Mutations in the highly conserved GGQ motif of class 1 polypeptide release factors abolish ability of human eRF1 to trigger peptidyl-tRNA hydrolysis. RNA *5*, 1014–1020.

Frolova, L., Seit-Nebi, A., and Kisselev, L. (2002). Highly conserved NIKS tetrapeptide is functionally essential in eukaryotic translation termination factor eRF1. RNA *8*, 129–136.

Gabriel, A., Dauvergne, F., Nolting, H.F., and Koch, M.H.J. (1994). Energy resolution using delay-line detectors. Nucl. Instrum. Methods Phys. Res. A *349*, 461–465.

Graille, M., Heurgué-Hamard, V., Champ, S., Mora, L., Scrima, N., Ulryck, N., van Tilbeurgh, H., and Buckingham, R.H. (2005). Molecular basis for bacterial class I release factor methylation by PrmC. Mol. Cell *20*, this issue, 917–927.

Heurgue-Hamard, V., Champ, S., Engstrom, A., Ehrenberg, M., and Buckingham, R.H. (2002). The hemK gene in *Escherichia coli* encodes the N(5)-glutamine methyltransferase that modifies peptide release factors. EMBO J. *21*, 769–778.

Heurgue-Hamard, V., Champ, S., Mora, L., Merkulova-Rainon, T., Kisselev, L.L., and Buckingham, R.H. (2005). The glutamine residue of the conserved GGQ motif in *Saccharomyces cerevisiae* release factor eRF1 is methylated by the product of the YDR140w gene. J. Biol. Chem. *280*, 2439–2445.

Ito, K., Uno, M., and Nakamura, Y. (2000). A tripeptide 'anticodon' deciphers stop codons in messenger RNA. Nature *403*, 680–684.

Jones, T.A., and Kjeldgaard, M. (1997). Electron-density map interpretation. Methods Enzymol. *277*, 173–208.

Kim, S.H., Sussman, J.L., Suddath, F.L., Quigley, G.J., McPherson, A., Wang, A.H., Seeman, N.C., and Rich, A. (1974). The general structure of transfer RNA molecules. Proc. Natl. Acad. Sci. USA *71*, 4970–4974.

Kisselev, L., Ehrenberg, M., and Frolova, L. (2003). Termination of translation: interplay of mRNA, rRNAs and release factors? EMBO J. *22*, 175–182.

Kjeldgaard, M. (2003). The unfolding story of polypeptide release factors. Mol. Cell *11*, 8–10.

Klaholz, B.P., Pape, T., Zavialov, A.V., Myasnikov, A.G., Orlova, E.V., Vestergaard, B., Ehrenberg, M., and van Heel, M. (2003). Structure of the *Escherichia coli* ribosomal termination complex with release factor 2. Nature *421*, 90–94.

Koch, M.H.J., and Bordas, J. (1983). X-ray diffraction and scattering on disordered systems using synchrotron radiation. Nucl. Instrum. Methods Phys. Res. A *208*, 461–469.

Koch, M.H., Vachette, P., and Svergun, D.I. (2003). Small-angle scattering: a view on the properties, structures and structural changes of biological macromolecules in solution. Q. Rev. Biophys. *36*, 147–227.

Konarev, P.V., Volkov, V.V., Sokolova, A.V., Koch, M.H.J., and Svergun, D.I. (2003). PRIMUS: a Windows PC-based system for small-angle scattering data analysis. J. Appl. Crystallogr. *36*, 1277–1282.

Kononenko, A.V., Dembo, K.A., Kiselev, L.L., and Volkov, V.V. (2004). Molecular morphology of eukaryotic class I translation termination factor eRF1 in solution. Mol. Biol. (Mosk.) *38*, 303–311.

Kozin, M.B., and Svergun, D.I. (2001). Automated matching of high- and low-resolution structural models. J. Appl. Crystallogr. *34*, 33–41.

Kurland, C.G., and Ehrenberg, M. (1987). Growth-optimizing accuracy of gene expression. Annu. Rev. Biophys. Biophys. Chem. *16*, 291–317.

Ma, B., and Nussinov, R. (2004). Release factors eRF1 and RF2: a universal mechanism controls the large conformational changes. J. Biol. Chem. *279*, 53875–53885.

Mora, L., Heurgue-Hamard, V., Champ, S., Ehrenberg, M., Kisselev, L.L., and Buckingham, R.H. (2003a). The essential role of the invariant GGQ motif in the function and stability in vivo of bacterial release factors RF1 and RF2. Mol. Microbiol. *47*, 267–275.

Mora, L., Zavialov, A., Ehrenberg, M., and Buckingham, R.H. (2003b). Stop codon recognition and interactions with peptide release factor RF3 of truncated and chimeric RF1 and RF2 from *Escherichia coli*. Mol. Microbiol. *50*, 1467–1476.

Ninio, J. (1974). A semi-quantitative treatment of missense and nonsense suppression in the strA and ram ribosomal mutants of *Escherichia coli*. Evaluation of some molecular parameters of translation in vivo. J. Mol. Biol. *84*, 297–313.

Pannekoek, Y., Heurgue-Hamard, V., Langerak, A.A., Speijer, D., Buckingham, R.H., and van der Ende, A. (2005). The N5-glutamine S-adenosyl-L-methionine-dependent methyltransferase PrmC/HemK in *Chlamydia trachomatis* methylates class 1 release factors. J. Bacteriol. *187*, 507–511.

Petoukhov, M.V., and Svergun, D.I. (2005). Global rigid body modeling of macromolecular complexes against small-angle scattering data. Biophys. J. *89*, 1237–1250.

Rawat, U.B., Zavialov, A.V., Sengupta, J., Valle, M., Grassucci, R.A., Linde, J., Vestergaard, B., Ehrenberg, M., and Frank, J. (2003). A cryo-electron microscopic study of ribosome-bound termination factor RF2. Nature *421*, 87–90.

Scolnick, E., Tompkins, R., Caskey, T., and Nirenberg, M. (1968). Release factors differing in specificity for terminator codons. Proc. Natl. Acad. Sci. USA *61*, 768–774.

Seit Nebi, A., Frolova, L., Ivanova, N., Poltaraus, A., and Kiselev, L. (2000). Mutation of a glutamine residue in the universal tripeptide GGQ in human eRF1 termination factor does not cause complete loss of its activity. Mol. Biol. (Mosk.) *34*, 899–900.

Seit-Nebi, A., Frolova, L., and Kisselev, L. (2002). Conversion of omnipotent translation termination factor eRF1 into ciliate-like UGA-only unipotent eRF1. EMBO Rep. *3*, 881–886.

Shin, D.H., Brandsen, J., Jancarik, J., Yokota, H., Kim, R., and Kim, S.H. (2004). Structural analyses of peptide release factor 1 from *Thermotoga maritima* reveal domain flexibility required for its interaction with the ribosome. J. Mol. Biol. *341*, 227–239.

Song, H., Mugnier, P., Das, A.K., Webb, H.M., Evans, D.R., Tuite, M.F., Hemmings, B.A., and Barford, D. (2000). The crystal structure of human eukaryotic release factor eRF1—mechanism of stop codon recognition and peptidyl-tRNA hydrolysis. Cell *100*, 311–321.

Suddath, F.L., Quigley, G.J., McPherson, A., Sneden, D., Kim, J.J., Kim, S.H., and Rich, A. (1974). Three-dimensional structure of yeast phenylalanine transfer RNA at 3.0 angstroms resolution. Nature *248*, 20–24.

Svergun, D.I. (1992). Determination of the regularization parameter in indirect-transform methods using perceptual criteria. J. Appl. Crystallogr. *25*, 495–503.

Svergun, D.I. (1999). Restoring low resolution structure of biological macromolecules from solution scattering using simulated annealing. Biophys. J. *76*, 2879–2886.

Svergun, D.I., Semenyuk, A.V., and Feigin, L.A. (1988). Small-angle-scattering-data treatment by the regularization method. Acta. Cryst. *44*, 244–250.

Svergun, D., Barberato, C., and Koch, M.H.J. (1995). CRYSOL—A program to evaluate X-ray solution scattering of biological macromolecules from atomic coordinates. J. Appl. Crystallogr. *28*, 768–773.

Vestergaard, B., Van, L.B., Andersen, G.R., Nyborg, J., Buckingham, R.H., and Kjeldgaard, M. (2001). Bacterial polypeptide release factor RF2 is structurally distinct from eukaryotic eRF1. Mol. Cell *8*, 1375–1382.

Yu, D., Ellis, H.M., Lee, E.C., Jenkins, N.A., Copeland, N.G., and Court, D.L. (2000). An efficient recombination system for chromosome engineering in *Escherichia coli*. Proc. Natl. Acad. Sci. USA *97*, 5978–5983.

Yusupov, M.M., Yusupova, G.Z., Baucom, A., Lieberman, K., Earnest, T.N., Cate, J.H., and Noller, H.F. (2001). Crystal structure of the ribosome at 5.5 Å resolution. Science *292*, 883–896.

Zavialov, A.V., Buckingham, R.H., and Ehrenberg, M. (2001). A post-termination ribosomal complex is the guanine nucleotide exchange factor for peptide release factor RF3. Cell *107*, 115–124.

Zavialov, A.V., Mora, L., Buckingham, R.H., and Ehrenberg, M. (2002). Release of peptide promoted by the GGQ motif of class 1 release factors regulates the GTPase activity of RF3. Mol. Cell *10*, 789–798.

Accession Numbers

The *Streptococcus mutans* coordinates are deposited by the Joint Center for Structural Genomics in the Protein Data Bank under accession number 1ZBT.